High Magnetic Shear Gain in a Liquid Sodium Stable Couette Flow Experiment: A Prelude to an $\alpha - \Omega$ Dynamo

Stirling A. Colgate,[1,2,*] Howard Beckley,[2,†] Jiahe Si,[2] Joe Martinic,[2] David Westpfahl,[2] James Slutz,[2] Cebastian Westrom,[2] Brianna Klein,[2] Paul Schendel,[2] Cletus Scharle,[2] Travis McKinney,[2] Rocky Ginanni,[2] Ian Bentley,[2] Timothy Mickey,[2] Regnar Ferrel,[2] Hui Li,[1] Vladimir Pariev,[1] and John Finn[3]

[1]*T-2, MS B-227, Los Alamos National Laboratory, Los Alamos, New Mexico 87545, USA*

[2]*Department of Physics, New Mexico Institute of Mining and Technology, Socorro, New Mexico 87801, USA*

[3]*T-5, Los Alamos National Laboratory, Los Alamos, New Mexico 87545, USA*

(Received 29 November 2010; published 28 April 2011)

The Ω phase of the liquid sodium α-Ω dynamo experiment at New Mexico Institute of Mining and Technology in cooperation with Los Alamos National Laboratory has demonstrated a high toroidal field B_ϕ that is $\simeq 8 \times B_r$, where B_r is the radial component of an applied poloidal magnetic field. This enhanced toroidal field is produced by the rotational shear in stable Couette flow within liquid sodium at a magnetic Reynolds number $\mathrm{Rm} \simeq 120$. Small turbulence in stable Taylor-Couette flow is caused by Ekman flow at the end walls, which causes an estimated turbulence energy fraction of $(\delta v/v)^2 \sim 10^{-3}$.

DOI: 10.1103/PhysRevLett.106.175003 PACS numbers: 47.65.Md, 52.72.+v

Major worldwide efforts are underway to understand astrophysical phenomena that depend upon magnetic fields, e.g., planetary, solar, and stellar magnetic fields, x rays, cosmic rays, TeV gamma rays, and jets and radio lobes powered by active galactic nuclei, and to interpret Faraday rotation maps of galaxy clusters. Yet, so far, there is no universally accepted explanation for the inferred large-scale magnetic fields. A process, called the $\alpha - \Omega$ dynamo [1–3], has been proposed which involves two orthogonal conducting fluid motions: shear and helicity. When the two motions are comparable, it is often described as a stretch, twist, and fold or ''fast'' dynamo and is claimed to be produced by turbulence alone [4,5]. The problem is that a turbulent dynamo must create these two orthogonal motions coherently from semirandom turbulent motions alone. Fluid turbulence causes the diffusion of magnetic flux as well as momentum [6], so that a field twisted one way by a turbulent eddy at one moment of time may be partially twisted the opposite way the next instant of time, leading to a net diffusion of magnetic flux [7].

A natural way to achieve a near unbounded multiplication of large-scale astrophysical magnetic flux is to use large-scale near-stable rotational shear flows (as in active galactic nuclei accretion disks and in stars) in combination with transverse, transient, rotationally coherent sources of helicity. The rotational shear flow can stretch and wind up an embedded, transverse magnetic flux through a large number of turns (the Ω effect, the subject of this Letter). When the winding number is large, the corresponding helicity, the α effect, can be correspondingly smaller in order to make positive dynamo gain. We have long believed that a unique source of coherent helicity is plumes [8,9] , driven by either star-disk collisions in active galactic nuclei [10] or large-scale (density scale height) convective elements in the base of the convective zone in stars [11]. In shear flows, turbulence is expected to be relatively small when stability is imposed by either an angular momentum gradient or an entropy gradient. The finite rotation of plumes [12], on the other hand, occurs because of the delayed turbulent mixing of the plume with the background matter. The necessary angle of rotation from toroidal to poloidal is $\pi/2$ rad, but, because of time-dependent diffusion of the plume with the background fluid, a measured absolute rotation of $\sim\pi$ rad results in a net rotation of the flux by $\sim\pi/2$ rad, ideal for the $\alpha - \omega$ dynamo.

In this experiment the high Ω gain in low-turbulence flow contrasts with a smaller Ω gain in higher turbulence shear flows. This result supports the ansatz that large-scale astrophysical magnetic fields can be created by semicoherent large-scale motions in which turbulence plays only a smaller, diffusive role that enables magnetic flux linkage.

Two liquid sodium dynamo experiments have produced positive exponential gain, but the flows were constrained by rigid walls unlike astrophysical flows [13,14]. The rigid walls restrict turbulent eddy size by the distance from the wall, according to the log-law of the walls [15], thereby producing lower turbulence. Three recent experiments used the Dudley-James [16] or von Karmán flows where both are counterrotating and converging flows at the midplane and are driven by either two counterrotating propellers or two counterrotating vaned turbine impellers, respectively [17–22]. Unconstrained turbulence is induced by the Helmholtz instability at the shearing midplane. This combination of coherent shearing motions and unconstrained shear-driven turbulence resulted in a maximum Ω gain of only unity [22]. Recognizing the enhanced resistivity of the midplane turbulence, the team at Wisconsin added a midplane baffle to reduce the turbulence, following which the Ω gain increased to $\simeq \times 4$ [7]. The von Kármán sodium 2 experiment in the same

geometry produced exponential gain [23]. However, the dynamo action was explained not by turbulence but primarily by the production of helicity by the large coherent vortices produced by the radial rigid vanes of the impeller [24]. (Ferromagnetism added additional gain to this source of helicity.)

The New Mexico $\alpha - \Omega$ dynamo experiment [25,26] is designed to explore the $\alpha\Omega$ possibility in the laboratory by using coherent fluid motions in low-turbulence, moderate shear, stable Couette flow in the annular volume between two coaxial cylinders, $R_2/R_1 = 2$ rotating at the stable angular velocities $\Omega_1/\Omega_2 = (R_2/R_1)^2 = 4$ (see Fig. 1). This is closely analogous to natural fluid motions that occur in astrophysical bodies [8,10,27]. The results of the first phase (Ω phase) of this two-phase experiment are presented here.

Besides the rotating Couette flow in the annular volume, Fig. 1 also indicates the Ekman flow, a thin fluid layer flowing along the boundaries of the annular volume. This flow is driven by fluid friction with the end walls whose surface rotates at $\Omega_2 < \Omega_{\text{fluid}}$. The Ekman flow produces both a torque and a small but finite level of turbulence [28] in the radial return flow. This turbulence adds a small turbulent resistivity to the resistivity of metallic sodium. The Ekman layer ($\Delta z \simeq R_1/\text{Re}^{1/2} = 4.08 \times 10^{-3}$ cm) flows "up" (towards the axis) along each end surface

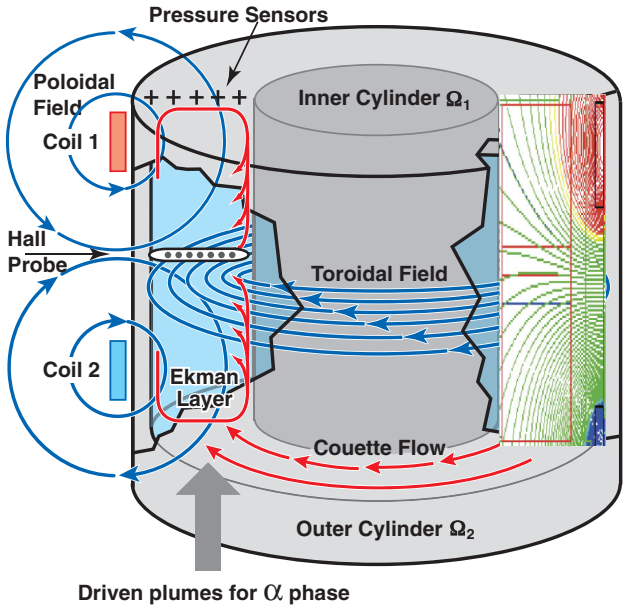

FIG. 1 (color). A schematic drawing of the fluid flow of the experiment shows the inner cylinder of $R_1 = 15.2$ cm rotating at $\Omega_1/2\pi = 68$ Hz relative to the outer or confining cylinder of $R_2 = 30.5$ cm and length $L = 30$ cm and $\Omega_2 = \Omega_1/4$ ($\Omega_2/2\pi = 17$ Hz). Liquid sodium in the annular space undergoes stable Couette rotational flow. The fluid Reynolds number is high: $\text{Re} = [(\Omega_1 + \Omega_2)/2][(R_2 + R_1)/2]^2/\nu = 1.35 \times 10^7$, $\nu = 10^{-2}$ cm^2/s. The magnetic Reynolds number becomes $\text{Rm} = \text{Re}(\nu/\eta_{\text{Na}}) = 180$ with $\eta_{\text{Na}} \sim 750$ cm^2/s.

and then radially back through the Couette flow to the outer cylinder R_2. Pressure sensors in the end wall and magnetic sensors within the magnetic probe housing are also shown schematically. The poloidal magnetic flux produced by two coils (left) is superimposed (right) showing the flux lines from the Maxwell calculation [29], with the ferromagnetic iron shield and steel shaft included. The magnetic flux of the radial field crosses the high shear of the liquid sodium Couette flow producing the enhanced toroidal field. The B_r field from the Maxwell calculations agrees with the calibrated probe measurements to 10%.

For the magnetic measurements 20 kW in an ac induction motor is used to drive stable Couette flow through a gear train with clutches and power takeoff that rotates the two cylinders at the fixed ratio of $\Omega_1 = 4\Omega_2$. The outer cylinder can also be disengaged from the gear train by a clutch, and a dc motor is used to accelerate or brake the outer cylinder independently from the driven inner cylinder. This allows different Ω_1/Ω_2 ratios to be explored. The dc motor housing (stator) is mounted on bearings. A torque arm with two force sensors connects the motor stator to ground, so that the torque on the dc motor can be measured separately from the drive of the inner cylinder. This arrangement allows us to measure the torque between the two cylinders due to the Ekman flow along the surface of the end plates which rotate more slowly at Ω_2. (The torque due to viscosity alone would be smaller by $1/\text{Re}^{1/2}$.)

In particular, when the inner cylinder is driven at higher speed by the ac motor, the Ekman fluid torque tries to spin up or accelerate the outer cylinder. Two torques counteract this acceleration: (i) the friction in the bearings that support the rotation of the outer cylinder and (ii) the torque on the dc motor when used as a generator or brake. In Fig. 2 (left), the crosses are the measurements of the braking force exerted by the dc motor torque arm; the dashed line is the calibrated bearing torque (measured by disengaging the inner cylinder drive and rotating the outer cylinder with the dc motor alone). The sum of these two torques is equal to the Ekman fluid torque spinning up the outer cylinder.

In Fig. 2 (left), the minimal Ekman flow torque G_{torq} occurs at $\Omega_1/\Omega_2 \simeq 3.25$, less than the limit of stable Couette flow of 4. The measured torque value is 2×10^8 dyne cm, close to the approximation that the torque equals the inward radial flux of angular momentum in the two Ekman layers [28] and at the radial velocity of $v_1/2$ and 2 layers. Therefore $G_{\text{torq}} = (\Delta_{\text{Ek}} 2\pi r_1)\Omega_1^2 r_1^3 = 2.37 \times 10^8$ dyne cm.

In Fig. 2 (right), the measured pressures are compared to the calculated pressures corresponding to two different angular velocity power laws. The upper (dashed) curve corresponds to ideal, maximum shear, stable Couette flow, or $\Omega \propto R^{-2}$, but the experimental points follow the lower solid curve corresponding to $\Omega \propto R^{-3/2}$. The Ekman flow torque has distorted the angular velocity profile and reduced the shear in the Couette volume relative to that of

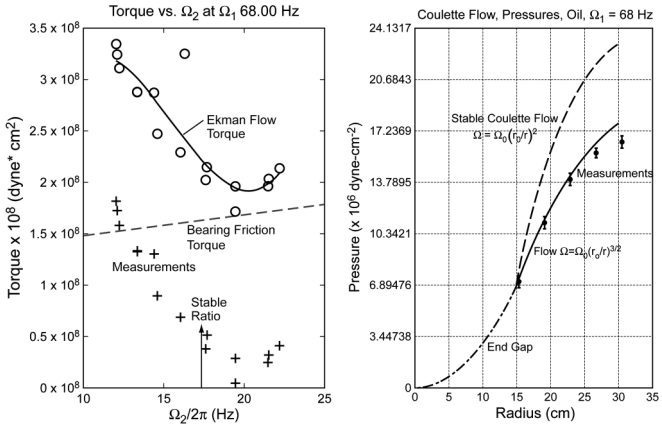

FIG. 2. (Left) Field-free fluid measurements have an absolute error of the order of 10%. The lower crosses are the measured dc generator torques; the dashed line is the measured bearings torque, and the sum of the two is the top solid curve, the torque due to the Ekman flow. (Right) Shown are the measured and theoretical pressure distributions. The pressure measurement starts at R_1 and extends to R_2. The finite pressure at R_1, $P_1 \simeq$ 100 psi, is due to the centrifugal pressure of rotating fluid in the narrow gap between the inner cylinder rotating at Ω_1 and the end wall rotating at Ω_2 (dot-dashed curve). This thin end gap is filled with rotating fluid, which extends from the shaft seal (where $P = 1$ atm) at radius $R_3 \simeq R_1/3$ to R_1, at which radius the Couette flow in the annular volume is initiated. From there, the two curves describe the pressure in the annular volume either extrapolated as $\Omega \propto R^{-2}$ or extrapolated as $R^{-3/2}$. The measurements fall along the $R^{-3/2}$ pressure distribution curve indicating less shear than the ideal Couette flow. The difference is presumed to be due to the torque produced by the Ekman flow.

the ideal Couette flow. High shear occurs in the thin boundary layers (with small Rm) in contact with the inner and outer cylinder walls.

Turbulent flow at such a high Reynolds number Re $\simeq 10^7$ is still well beyond current simulation capability, and so simulations can be performed only at a greatly reduced Re. The Ekman flow is a flux of fluid of reduced angular momentum deposited at the inner cylinder whose torque is measured. The torque producing this angular momentum is friction with the end walls, which in turn reduces the angular velocity of the Couette flow in the annular volume. Unstable flow, turbulent friction with the inner cylinder surface, counteracts this torque by speeding up this flow. An approximate turbulent solution is that the torque in the Couette volume is a constant, independent of radius and axial position. Then this shear stress is maintained constant in two laminar sublayers with Re $\simeq 100$ and in two turbulent boundary layers in a log-law-of-the-walls solution. When the distance from the walls corresponds to an eddy scale of the radial gradient, a transition takes place to a scale-independent eddy size turbulent torque connecting the two regions at inner and outer boundaries. The mean velocity distribution in the above analysis gives a reduced shear $\Omega/\Omega_1 \propto (R_1/R)^{1.64}$, compared to the value $\Omega/\Omega_1 \propto (R_1/R)^{1.5}$ derived from the pressure distribution of Fig. 2 and the ideal Couette flow ratio $\Omega/\Omega_1 \propto (R_1/R)^2$.

Figure 1 also shows the magnetic field configuration. The magnetic field Hall detector probe, internal to the liquid sodium at the midplane, is the primary diagnostic of the experiment. It consists of 6 multiple, 3-axis, magnetic field Hall effect detectors at the midplane in the annular space between the two cylinders and contained in an aerodynamically shaped housing. (The fluid friction drag produced by this housing, primarily Ekman flow, is estimated to be ~0.1 of the end-wall Ekman torque.) The Ω gain was then measured by using an applied calibrated B_r magnetic field as a function of the coil currents. Because of the high gain in B_ϕ and the lack of perfect orthogonality of the Hall detectors, the measured B_r would be expected to be contaminated by a small fraction of the much larger B_ϕ field.

Figure 3 confirms that the measurements are repeatable by showing four experiments overlaid, but the absolute error is ~10%. The Ω-gain ratio of $\times 8$ is repeated with a low bias field of $B_r \simeq 12$ G. The time variation between each run reflects slight changes in the measurement time relative to the Couette flow relaxation time and, hence, the angular velocity distribution. The repeatability as well as several earlier runs in the previous six months gives us confidence that the conclusion of high Ω gain is valid. Note that the ideal Ω gain could be as high as $\sim R_m/2\pi \simeq \times 20$ [8], but several factors contribute to a reduced gain. (i) The reduced shear $d\Omega/dR \simeq 1.5$ rather than 2, a factor of 0.75. (ii) The geometry of the current flow is now two directions, reentrant rather than the "ideal" single direction, a factor

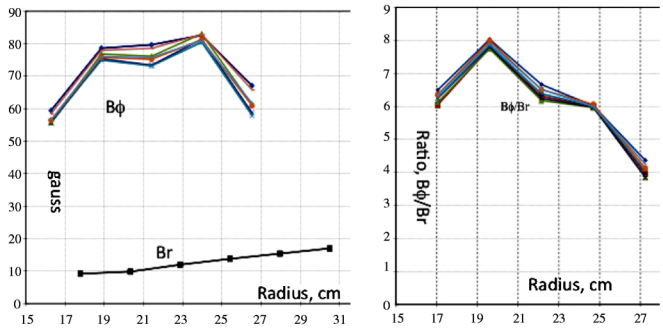

FIG. 3 (color online). (Left) The lower curve, left, shows the applied radial magnetic field $B_r \simeq 12$ G, and the upper curve the resulting toroidal field for four overlaid experiments at $\Omega_1/2\pi = 68$ Hz. The backreaction of this toroidal stress is small: $B_R B_\phi/8\pi \simeq 1.7 \times 10^{-2}\tau_{\mathrm{Ek}}$, where the stress per unit area in the fluid due to the Ekman flow τ_{Ek} becomes (measured torque: 2×10^8 dyne cm)/(area $\times$ torque arm). $\tau_{\mathrm{Ek}} \simeq 2.6 \times 10^3$ dyne/cm^2. The upper curves show the measured toroidal magnetic field for four overlaid experiments at $\Omega_1/2\pi = 68$ Hz. The right panel shows the ratio B_ϕ/B_r with a maximum of $\times 8$ with an error of ~10% at $\sim(R_2 - R_1)/3 \simeq$ 5 cm from the inner cylinder wall.

of ~0.5. (iii) In addition, the current must flow radially from an inner to an outer annulus of conducting sodium. The resistance of this additional current path further reduces the effective gain. (iv) Finally, we estimate the effective resistivity of the Ekman driven turbulence and find it modest compared to the sodium.

In the caption of Fig. 3, the Ekman turbulent stress is estimated to be $\tau_{\mathrm{Ek}} \simeq 2.6 \times 10^3$ dyne/cm^2, and so the turbulent fluid velocities become $v_t \sim (\tau_{\mathrm{Ek}}/\rho)^{1/2} \simeq 51$ cm/s. The turbulent diffusivity is $\eta_t = v_t \lambda/3$, where λ is the largest effective eddy size $\lambda \sim (R - 2 - R_1)/3 = 5$ cm, and so $\eta_t \simeq 83$ cm^2/s as compared to hot liquid sodium of $\eta_{\mathrm{Na}} \simeq 750$ cm^2/s or only a 9% increase in resistivity.

The expected backreaction is observed when the radial component of the applied poloidal field is increased from $\simeq 12$ to $\simeq 250$ G. This results in an added torque between the cylinders producing additional current and torque in the drive motor, $\sim \times 1.5$. The Ω-gain ratio is reduced from $\times 8$ to $\simeq \times 3$. The observed delay of several seconds for the backreaction torque to reach equilibrium is presumably the spin-down time for the Couette flow to reach a new, modified velocity profile. The backreaction stress $B_R B_\phi/8\pi \simeq 7.7\tau_{\mathrm{Ek}}$ is consistent with the assumption that this stress reduces the shear in the Couette flow and hence reduces the Ω gain. The pressure distribution and, hence, the inferred Couette flow angular velocity distribution has yet to be measured. In order to estimate the difference in applied power, $\simeq 10$ kW, the specific magnetic field energy density $B_\phi^2/8\pi$ is dissipated at $\langle\Omega\rangle \times (\mathrm{Vol})$, where the volume of high B_ϕ is estimated as $(\mathrm{Vol}) \simeq (L/3)(\pi/2) \times (R_2^2 - R_1^2)$. This results in a power of $\simeq 8$ kW, roughly consistent with the measured increase in power of 10 kW.

A large Ω gain in low turbulent shear flow in a conducting fluid is demonstrated. This is likely to be the mechanism of the Ω gain of a coherent $\alpha - \Omega$ astrophysical dynamo. This experiment has been funded by NSF, University of California, NMIMT, and LANL.

*colgate@lanl.gov
†Deceased.

[1] E. N. Parker, Astrophys. J. **121**, 29 (1955).
[2] F. Krause and K. H. Rädler, *Mean-Field Magnetohydrodynamics and Dynamo Theory* (Pergamon, Oxford, 1980).
[3] E. N. Parker, *Cosmical Magnetic Fields, Their Origin and Their Activity* (Clarendon, Oxford, 1979).
[4] A. Nordlund *et al.*, Astrophys. J. **392**, 647 (1992).
[5] Ya. B. Zeldovich, A. A. Ruzmaikin, and D. D. Sokoloff, *Magnetic Fields in Astrophysics* (Gordon and Breach, New York, 1983).
[6] S. M. Tobias and F. Cattaneo, Phys. Rev. Lett. **101**, 125003 (2008).
[7] K. Rahbarnia *et al.*, Bull. Am. Phys. Soc. **NP9-73**, 218 (2010).
[8] V. I. Pariev, S. A. Colgate, and J. M. Finn, Astrophys. J. **658**, 129 (2007).
[9] G. T. Willette, Ph.D. thesis, Cal Tech, 1994.
[10] V. I. Pariev and S. A. Colgate, Astrophys. J. **658**, 114 (2007).
[11] L. Mestel, *Stellar Magnetism* (Clarendon, Oxford, 1999).
[12] H. F. Beckley, S. A. Colgate, V. D. Romero, and R. Ferrel, Astrophys. J. **599**, 702 (2003).
[13] A. Gailitis *et al.* Phys. Rev. Lett. **84**, 4365 (2000).
[14] R. Stieglitz and U. Müller, Phys. Fluids **13**, 561 (2001).
[15] L. D. Landau and E. M. Lifshitz, *Fluid Mechanics* (Pergamon, London, 1959).
[16] M. L. Dudley and R. W. James, Proc. R. Soc. A **425**, 407 (1989).
[17] C. B. Forest, R. A. Bayliss, R. D. Kendrick, M. D. Nornberg, R. O'Connell, and E. J. Spence, Magnetohydrodynamics **38**, 107 (2002).
[18] D. L. Lathrop, W. L. Shew, and D. R. Sisan, Plasma Phys. Controlled Fusion **43**, A151 (2001).
[19] P. Odier, J.-F. Pinton, and S. Fauve, Phys. Rev. E **58**, 7397 (1998).
[20] N. L. Peffley, A. B. Cawthorne, and D. P. Lathrop, Phys. Rev. E **61**, 5287 (2000).
[21] F. Petrelis, M. Bourgoin, L. Marie, J. Burguete, A. Chiffaudel, F. Daviaud, S. Fauve, P. Odier, and J.-F. Pinton, Phys. Rev. Lett. **90**, 174501 (2003).
[22] E. J. Spence, M. D. Nornberg, C. M. Jacobson, C. A. Parada, N. Z. Taylor, R. D. Kendrick, and C. B. Forest, Phys. Rev. Lett. **98**, 164503 (2007).
[23] R. Monchaux *et al.*, Phys. Rev. Lett. **98**, 044502 (2007).
[24] R. Laguerre, C. Nore, A. Riberiro, J. L. Guermond, and F. Plunian, Phys. Rev. Lett. **101**, 104501 (2008).
[25] S. A. Colgate, Astron. Nachr. **327**, 456 (2006).
[26] S. A. Colgate, V. I. Pariev, H. F. Beckley, R. Ferrel, V. D. Romero, and J. C. Weatherall, Magnetohydrodynamics **38**, 129 (2002).
[27] A. Brandenburg, in *Theory of Black Hole Accretion Disks*, edited by M. A. Abramowicz, G. Bjornsson, and J. E. Pringle (Cambridge University Press, Cambridge, England, 1998).
[28] H. Ji, J. Goodman, and A. Kageyama, Mon. Not. R. Astron. Soc. **325**, L1 (2001).
[29] Ansoft Maxwell Corporation, http://www.ansoft.com/, 1980.